



Basalts and picrites from a plume-type ophiolite in the South Qilian Accretionary Belt, Qilian Orogen: Accretion of a Cambrian Oceanic Plateau?

Yuqi Zhang^a, Shuguang Song^{a,*}, Liming Yang^a, Li Su^b, Yaoling Niu^{c,d}, Mark B. Allen^c, Xin Xu^a

^a MOE key Laboratory of Orogenic Belt and Crustal Evolution, School of Earth and Space Sciences, Peking University, Beijing 100871, China

^b Institute of Earth Science and State Key Laboratory of Geological Processes and Mineral Resources, Chinese University of Geosciences, Beijing 100083, China

^c Department of Earth Sciences, Durham University, Durham DH1 3LE, UK

^d Institute of Oceanology, Chinese Academy of Science, Qingdao 266071, China

ARTICLE INFO

Article history:

Received 14 October 2016

Accepted 28 January 2017

Available online 08 February 2017

Keywords:

Picrites

Cambrian oceanic plateau

Trench jam

South Qilian accretionary belt

Qilian Orogen

ABSTRACT

Oceanic plateaus with high-Mg rocks in the present-day oceanic crust have attracted much attention for their proposed mantle-plume origins and abnormally high mantle potential temperatures (T_p). However, equivalent rocks in ancient oceanic environments are usually poorly preserved because of deformation and metamorphism. Here we present petrological, geochronological and geochemical data for pillow lavas from Cambrian ophiolites in the Lajishan and Yongjing regions of the South Qilian Accretionary Belt (SQAB), from the southern part of the Qilian Orogen, northern China. Three rock groups can be identified geochemically: (1) sub-alkaline basalts with enriched mid-ocean ridge basalt (E-MORB) affinity; (2) alkaline basalts with oceanic island basalt (OIB) features, probably derived from partial melting of an enriched mantle source; and (3) picrites with MgO (18–22 wt%). Cr-numbers [$Cr^\# = Cr/(Cr + Al)$] of spinels from the picrites suggest 18–21% degree of partial melting at the estimated mantle potential temperature (T_p) of 1489–1600 °C, equivalent to values of Cenozoic Hawaiian picrites (1500–1600 °C). Zircons from one gabbro sample yielded a U–Pb Concordia age of 525 ± 3 Ma, suggesting the oceanic crust formed in the Cambrian. Available evidence suggests that Cambrian mantle plume activity is preserved in the South Qilian Accretionary Belt, and influenced the regional tectonics: “jamming” of the trench by thick oceanic crust explains the emplacement and preservation of the oceanic plateau, and gave rise to the generation of concomitant Ordovician inner-oceanic island arc basalts via re-organisation of the subduction zones in the region.

© 2017 Elsevier B.V. All rights reserved.

1. Introduction

Most volcanism in ocean basins occurs at plate boundaries: mid-ocean ridges and subduction zones. In contrast, the rocks of oceanic plateaus, oceanic islands and seamounts are different from the plate margin magmatism in composition (e.g., Kerr et al., 1996a, 1996b). Although these intraplate igneous rocks only represent <1% of all igneous rocks on Earth, great emphasis has been placed on them because they provide insights into mantle composition, magma formation processes and magma evolution (Greenough et al., 2005). Oceanic plateaus represent an enormous transfer of magma from the mantle to crust, mostly as submarine large igneous provinces (LIPs) (>100,000 km²) (Coffin and Eldholm, 1994; Condie, 2001). Most of the oceanic plateaus formed in a span of a few million years, suggesting immense volcanic eruptions with global impact related to continental break-up (Coffin

and Eldholm, 1992; Kerr and Mahoney, 2007). The origin of oceanic islands has been debated throughout the development of plate tectonic theory, but the most popular opinion is still “hot spot” or mantle plume, which is consistent with the geochemical features of oceanic island volcanic rocks (Hofmann and White, 1982; Morgan, 1971).

Since the term “komatiite” was first introduced to describe the spinifex-textured MgO-rich lavas in the Barberton area, South Africa (Viljoen and Viljoen, 1969), it has attracted considerable interest in the geochemical community. High-Mg lavas without a spinifex texture are known as picrites, and the occurrence of both komatiites and picrites in post-Archean times indicate a hotter than normal mantle origin (mantle potential temperature, $T_p \sim 1450$ –1600 °C), and thus a higher degree of melting is needed for their formation (e.g., Arndt et al., 1997; Kerr et al., 1996a, 1996b; Shimizu et al., 2001). Their origin has a close affinity with the activity of mantle plumes (Herzberg and Asimow, 2015; Herzberg and Hara, 2002; Herzberg et al., 2007). Picrites and komatiites (e.g., Kerr and Arndt, 2001; Le Bas, 2000), are relatively rare in Earth history and generally are associated with LIPs caused by

* Corresponding author.

E-mail address: sgsong@pku.edu.cn (S. Song).

the melting of large hot plumes from the deep mantle (e.g., [Campbell and Griffiths, 1990](#); [Kerr et al., 1996b](#); [Richards et al., 1989](#)).

In this paper, we present detailed petrological and geochemical data of the volcanic rocks from the Lajishan and Yongjing ophiolites (LYO) of the South Qilian Accretionary Belt (SQAB), Qilian Orogen. We have determined that the LYO sequences are products of a fragmented ocean plateau generated in the Cambrian (~525 Ma), and provide the first evidence for the activity of a mantle plume preserved in northwestern China at this time. In addition, we propose an accretionary mechanism by “trench jam” of plateau rocks in the subduction zone.

2. Regional geology

The Qilian orogenic belt, presently exposed at the northern margin of the Qinghai-Tibetan Plateau, northwestern China is part of the Qinling–Qilian–Kunlun Fold System (e.g., [Jiang et al., 2000](#)). It is situated at a triple junction between the North China Craton (NCC), the Yangtze Craton (YC) and the Tarim Craton (TC) in the northwest ([Fig. 1](#)).

The whole Qilian–Qaidam region consists of two oceanic accretionary belts and one continental-type ultra-high pressure metamorphic (UHPM) belt, juxtaposed with two Precambrian blocks, from north to south, (1) the North Qilian Accretionary Belt, (2) the Central Qilian Block, (3) the South Qilian Accretionary Belt, (4) the Quanji Block and (5) the North Qaidam UHPM Belt ([Fig. 1](#)).

The North Qilian Accretionary Belt (NQAB) extends for ~1000 km northwest-southeast, and is offset by the sinistral, active, strike slip Altyn Tagh Fault for up to 400 km ([Zhang et al., 2001](#)). In the northeast, the Alashan block is bounded by the Longshoushan Fault (LF), and considered to be the westernmost component of the NCC ([Zhang et al., 2013](#); [Zhao and Cawood, 2012](#)). The Central Qilian block in the south is bounded to its northeast by the North Margin Fault (NMF) and has a Precambrian basement, which has affinities with the Yangtze block. ([Song et al., 2010a, 2012, 2013](#); [Tung et al., 2007, 2013](#); [Wan et al., 2001](#)). The North Qaidam UHPM belt represents a continent-continental collision zone along the northern margin of the Qaidam Basin ([Song et al., 2014](#)).

The North Qilian Accretionary Belt records globally one of the earliest “cold” oceanic subduction zones, in response to the closure of the ancient Qilian Ocean between the Alashan and Qilian–Qaidam blocks during the Early Paleozoic ([Song et al., 2006, 2007, 2009, 2013](#); [Wu et al., 1993](#); [Xiao et al., 2009](#); [Yin et al., 2007](#); [Zhang et al., 2007](#)). It consists of Precambrian basement, Early Paleozoic subduction-related rock associations (ophiolite complexes, high-pressure/ low-temperature metamorphic rocks, arc-related volcanic and intrusive rocks), Silurian flysch and Devonian molasses formations, and later sedimentary cover ([Song et al., 2013](#)). The Qilian Block is a thrust belt of slices of Precambrian basement, overlain by Paleozoic sedimentary sequences. The basement consists of granitic gneiss, marble, amphibolite and minor granulite with ages of 880–940 Ma ([Tung et al., 2007](#); [Wan et al., 2001](#)), similar to ages of the granitic gneisses in the North Qaidam UHPM Belt ([Song et al., 2012](#)).

The South Qilian Accretionary Belt (SQAB) occurs as discontinuous fault-bound slivers along a NW–SE orientation between the Central Qilian and Quanji blocks, in parallel to the North Qilian Accretionary Belt ([Fig. 1](#)). From NW to SE, this belt consists of the Yanchiwan Terrane, the Gangcha Terrane, the Lajishan Terrane and the Yongjing Terrane, in total around 1000 km in length ([Fig. 1](#)). The accretionary belt is composed of two sequences: the ophiolite sequence and the arc-volcanic sequence; no high-pressure metamorphic rocks have been found in these areas. The arc-volcanic sequence consists of mafic to intermediate volcanic rocks of Ordovician age (460–440 Ma), in which forearc boninite has also been reported ([Yang et al., 2002](#); [Song et al., unpublished data](#)). Compositions suggest that they formed in an intra-oceanic arc environment; boninites have also been reported in this belt, interpreted as having a forearc origin ([Yang et al., 2002](#)). Most of the ophiolite rocks crop out in the north relative to the arc sequence ([Fig. 1](#)), and they consist of ultramafic rocks (pyroxenite and dunite), gabbros, massive and pillow basalts and pelagic chert.

3. Rock assemblages and petrography

The Lajishan Ophiolite occurs as a narrow terrane occupying an area of ~150 × 75 km², between the two thrust faults of the NW–SE

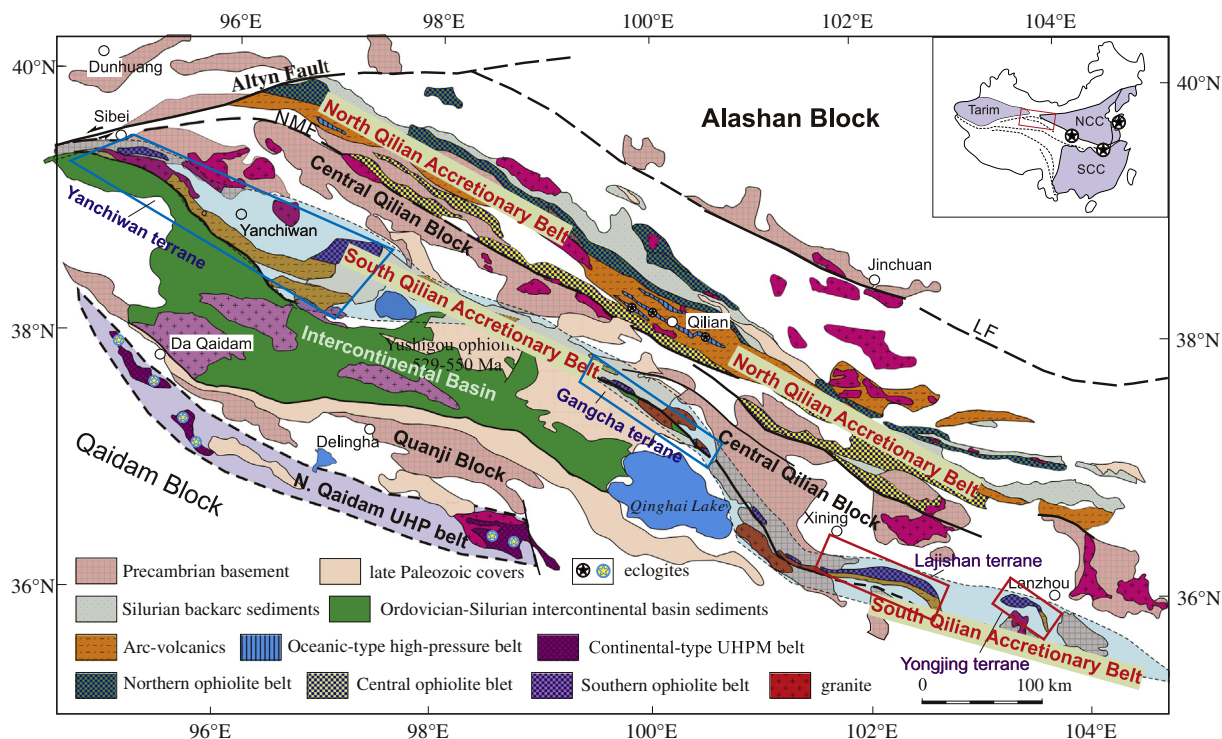


Fig. 1. Simplified geological map of the Qilian–Qaidam orogens showing two accretionary belts (North Qilian and South Qilian accretionary belts) and the localities (red rectangles) of the Lajishan and Yongjing ophiolites of this study. (For interpretation of the references to colour in this figure legend, the reader is referred to the web version of this article.)

orientation. To its south are the Ordovician arc-volcanic sequences. The ophiolite is composed of voluminous mafic volcanic rocks (pillow and massive lavas/dykes) associated with minor pelagic sedimentary rocks such as the red radiolarian chert (Fig. 2a and b). Mafic to ultramafic rocks from the basal part of the ophiolite suite are sporadically scattered within the terrane, including serpentinised mantle harzburgite, cumulate peridotite and pyroxenite. Basaltic rocks occur mainly as pillow basalts that have been interpreted as thin submarine flows.

The Yongjing Ophiolite mainly consists of massive and pillow basalts and two small serpentinised ultramafic bodies. The massive basalts have a green colour and occur as thick layered lavas without columnar jointing, which probably represent the thick lava flows of fast eruption

(Aitken and Echeverría, 1984). Some outcrops look like sheeted dykes with nested chilled margins (Fig. 2c). The pillow basalts have a dark-green colour, and overlap onto the massive basalts (Fig. 2d); some pillow lavas are slightly deformed (Fig. 2e).

Picrites in the Yongjing Ophiolite are dark-coloured lavas with pillowed structure (Fig. 2f and g), except for the massive sample 13QLS-137. They have experienced ocean floor alteration with the development of the typical mineral assemblage of low-grade greenschist facies conditions. All the olivines have been altered to chlorite or serpentinite (Fig. 3a, b), and pyroxene has altered to tremolite (Fig. 3a). Subalkaline basalts possess conspicuous ophitic textures with plagioclase serving as the frame and clinopyroxene filling into

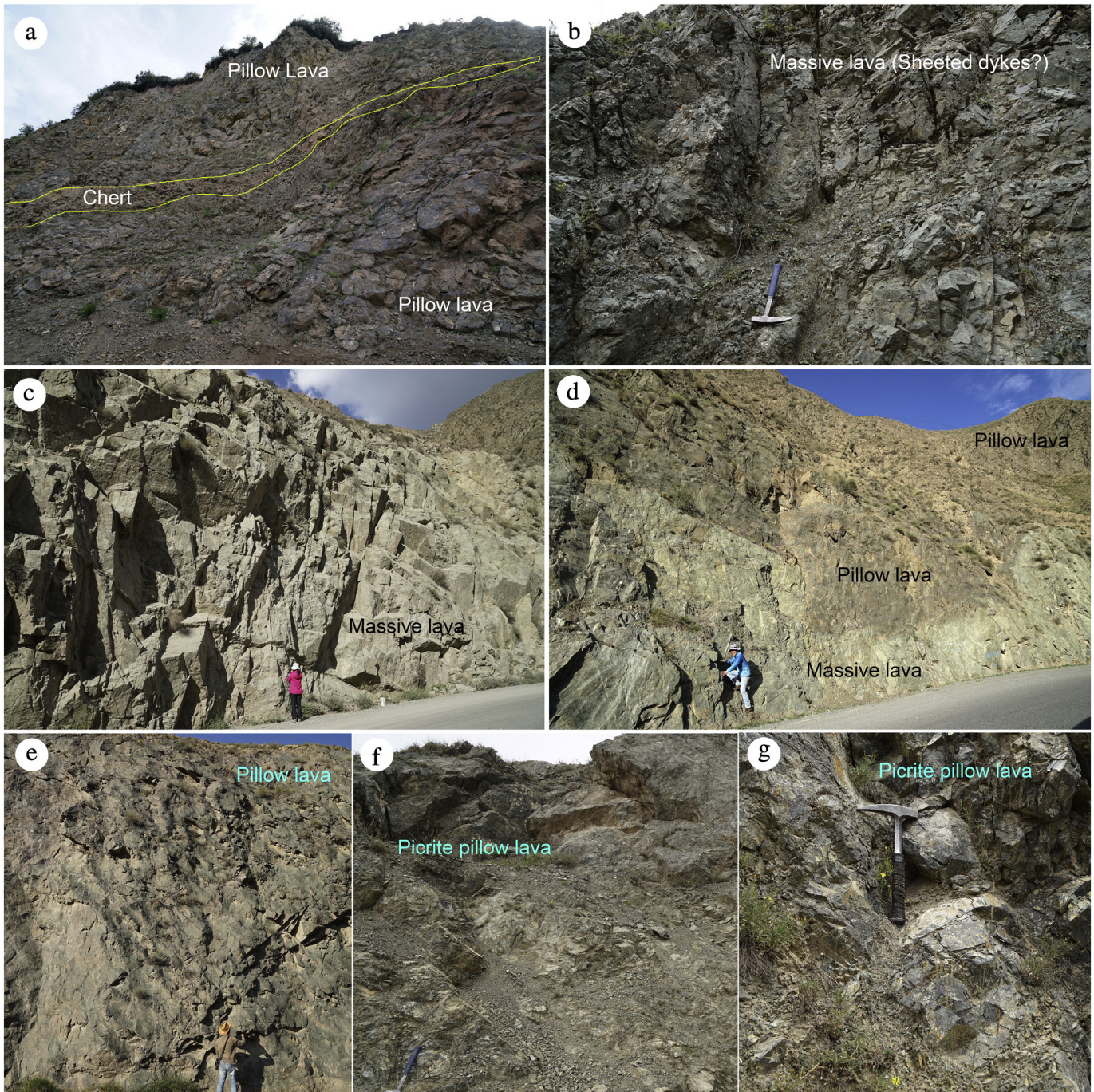


Fig. 2. Field photos of the Lajishan–Yongjing ophiolite terranes. (a) Pillow basalts with red chert in the Lajishan locality. (b) Massive lavas (sheeted dykes?) in the Lajishan locality. (c) Voluminous massive lava in the Yongjing locality. (d) and (e) Pillow lava overlaying the massive lavas in the Yongjing locality. (f) and (g) Picrites with pillow structure. (For interpretation of the references to colour in this figure legend, the reader is referred to the web version of this article.)

the gaps in between (Fig. 3c). Flow structure occurs in some alkaline basalts (Fig. 3d). Some rocks with high-Cr composition also contain chrome spinels (Fig. 3a, d).

4. Analytical methods and results

4.1. Analytical methods

4.1.1. Bulk rock major and trace element analysis

Bulk-rock major element oxides (SiO_2 , TiO_2 , Al_2O_3 , FeO , MnO , MgO , CaO , Na_2O , K_2O , and P_2O_5) were determined using inductively coupled plasma-optical emission spectroscopy (ICP-OES) at China University of Geosciences, Beijing (CUGB). The analytical precisions (1σ) for most major elements based on rock standards AGV-2 (US Geological Survey), GSR-1, GSR-3 and GSR-5 (National geological standard reference materials of China) are better than 1% with the exception of TiO_2 (~1.5%) and P_2O_5 (~2.0%). Loss on ignition (LOI) was determined by placing 1 g of samples in the furnace at 1000 °C for several hours before being cooled in a desiccator and reweighed (Song et al., 2010b).

The trace element analysis for Lajishan basaltic samples were performed on an Agilent-7500a inductively coupled plasma mass spectrometer (ICP-MS) in the Institute of Earth Science of CUGB. About 40 mg of sample powder was dissolved in equal mixture of sub-boiling distilled HNO_3 and HF with a Teflon digesting vessel on a hot-plate at 185 °C for 48 h using high-pressure bombs for digestion/dissolution. The samples were then evaporated to incipient dryness, refluxed with 6 N HNO_3 , and heated again to incipient dryness. The sample was again dissolved in 2 mL of 3 N HNO_3 in high-pressure bombs for a further 24 h to ensure complete dissolution. Such digested samples were

diluted with Milli-Q water to a final dilution factor of 2000 in 2% HNO_3 solution with total dissolved solid of 0.05%. Precisions (1σ) for most elements based on liquid standards Std-1, Std-2, Std-4 (AccuStandard, USA). Rock standards AGV-2 (US Geological Survey), and GSR-1, GSR-3, GSR-5 (National geological standard reference materials of China) were used to monitor the analytical accuracy and precision. The analytical accuracy, as indicated by relative difference between measured and recommended values, is better than 5% for most elements, and 10–15% for Cu, Zn, Gd and Ta.

4.1.2. Bulk rock Sr–Nd isotope analysis

The bulk-rock Sr–Nd isotope analysis was done at Key Laboratory of Orogenic Belts and Crustal Evolution, Peking University. The pure Sr and Nd were obtained by passing through conventional cation columns (AG50W and P507) for analysis using a multi-collector inductively coupled plasma mass spectrometer (MC-ICP-MS) of the type VG AXIOM. Mass fractionation corrections for Sr and Nd isotopic ratios were normalised to $^{86}\text{Sr}/^{88}\text{Sr} = 0.1194$ and $^{146}\text{Nd}/^{144}\text{Nd} = 0.7219$, respectively.

4.1.3. In-situ zircon U–Pb dating

Zircons were separated from gabbroic sample 12LJ26 by using standard density and magnetic separation techniques and purified by hand-picking under a binocular microscope. The Cathodoluminescence (CL) examination was done by using an FEI QUANTA650 FEG Scanning Electron Microscope (SEM) under conditions of 15 kV/120 nA in the School of Earth and Space Sciences, Peking University, Beijing.

Measurements of U, Th and Pb in zircons were carried out on an Agilent-7500a quadrupole inductively coupled plasma mass

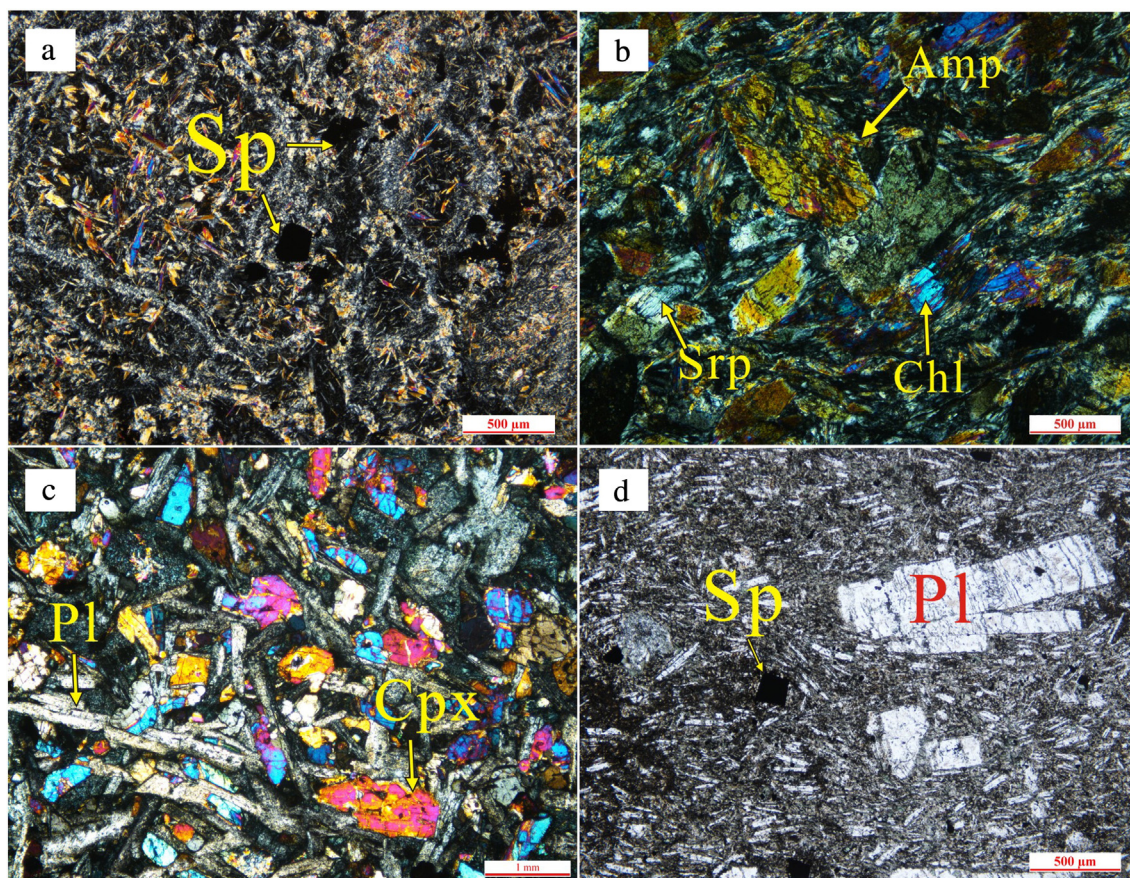


Fig. 3. Photomicrographs of pillow and massive lavas and picrites. (a) Pillowed picrites with high MgO have experienced low-grade metamorphism. Olivine is metamorphosed to serpentine and pyroxene is altered to tremolite (sample LJ15-176); (b) the massive picrite possesses amphibole metacrystals that may result from retrogressive metamorphism. Olivine is metamorphosed to serpentine and chlorite (sample 13QLS-137); (c) sub-alkaline basalt showing conspicuous intersertal and ophitic texture (sample 13QLS-78); (d) alkaline basalts showing flow structure with orthopyroxene and spinel phenocryst (sample 13QLS-98).

spectrometry coupled with a New Wave SS UP193 laser sampler (LA-ICP-MS) at CUGB. Laser spot size of 36 μm , laser energy density of 8.5 J/cm² and a repetition rate of 10 Hz were applied for analysis (see Song et al., 2010b for more details). Age calculations and plots of Concordia diagrams were done using Isoplot (Ludwig, 2003).

4.2. Geochemical feature of Lajishan basalts

4.2.1. Whole-rock major and trace element analysis

The analysed samples are predominantly basaltic and present large ranges of MgO and total alkali (Na₂O + K₂O) contents (Table 1 and Appendix Table 1). In the (Nb/Y)–(Zr/TiO₂) diagram (Winchester and Floyd, 1976), some samples plot in the alkaline field, while others are in the subalkaline field (Fig. 4a). Six pillow basalt samples and one massive basalt sample (13QLS-137) from the Yongjing Ophiolite have very high MgO contents (>18 wt%). All the picritic pillow basalts plot in the alkaline field of the (Nb/Y)–(Zr/TiO₂) diagram with high Ti/Y ratios more than 500, except for the massive basaltic sample 13QLS-137 (Fig. 4a). Therefore, according to these geochemical features, we can

subdivide these basaltic samples into three groups: (1) the sub-alkaline group, (2) the alkaline group and (3) picrite group.

- (1) Sub-alkaline basalts. This group of basalts are characterised by relatively low TiO₂, Nb, Ni, Zr, but high Yb and V relative to alkaline basalts (Fig. 5); they have sub-alkaline, tholeiitic compositions; major element characteristics are more variable (Fig. 4). They also have low Nb/Y and Ti/Y (mostly < 500), very different from the alkaline basalts. They possess slight enrichment of LREE and MREE, with (La/Yb)_N ranging from 1.24 to 4.45 and (Sm/Yb)_N from 1.19 to 2.58. The REE and trace element patterns illustrate that these rocks are similar to typical present-day enriched E-MORB (Fig. 6a, b).
- (2) Alkaline basalts. The alkaline basalts display MREE/HREE and LREE/HREE enriched patterns. They have higher Nb/Y (0.76–2.32) and Ti/Y (mostly > 500) than the sub-alkaline basalts. The overall geochemical features of these basalts resemble those of alkaline basalts generated at within-plate oceanic island settings (Fig. 6c, d), as also exemplified by the relatively high Ti/V (~50), their Th/Yb–Ta/Yb ratios as well as other most common

Table 1

Representative major and trace element analyses of basalts from Lajishan-Yongjing ophiolites.

Sample	12LJ-19	12LJ-20	13QLS114	13QLS128	LJ15-173	LJ15-177	12LJ-28	12LJ-29	13QLS-115	13QLS-137	LJ15-174	LJ15-175
Rock	SAB	SAB	SAB	SAB	AB	AB	AB	AB	Picrite	Picrite	Picrite	Picrite
Location	LJS	LJS	YJ	YJ	YJ	YJ	LJS	LJS	YJ	YJ	YJ	YJ
<i>Major elements (wt%)</i>												
SiO ₂	49.64	51.54	45.78	45.77	48.96	47.89	47.10	46.11	46.58	49.93	44.11	46.08
TiO ₂	1.08	1.03	2.76	1.65	1.82	1.68	1.69	1.61	1.46	0.52	1.54	1.16
Al ₂ O ₃	13.62	13.96	14.57	13.98	13.88	13.94	11.46	10.68	7.92	9.37	7.06	5.88
Fe ₂ O ₃ T	11.70	11.40	15.91	9.09	11.49	11.67	11.05	11.66	12.67	9.26	12.57	11.69
MnO	0.18	0.20	0.22	0.17	0.17	0.22	0.13	0.11	0.17	0.26	0.19	0.17
MgO	7.06	7.21	4.39	5.72	7.40	8.11	5.98	4.85	19.76	17.72	21.06	21.47
CaO	9.67	7.23	9.95	10.24	10.23	8.36	9.52	10.26	7.80	7.69	8.02	8.20
Na ₂ O	3.81	4.54	3.39	2.80	3.99	3.84	3.36	3.33	0.30	0.97	0.31	0.26
K ₂ O	0.08	0.20	0.75	1.38	0.33	1.00	0.85	0.64	0.03	0.21	0.04	0.03
P ₂ O ₅	0.10	0.08	0.49	0.29	0.19	0.20	0.41	0.42	0.14	0.22	0.15	0.10
LOI	2.20	1.71	2.13	7.83	0.69	2.17	7.66	9.54	2.42	3.02	3.68	3.77
Total	99.13	99.11	100.33	98.92	99.14	99.07	99.23	99.21	99.24	99.16	98.73	98.82
Mg#	58.45	59.57	39.13	59.46	60.02	61.84	55.79	49.25	78.42	81.68	79.61	81.06
<i>Trace elements (ppm)</i>												
Sc	46.06	42.46	27.98	38.84			21.16	20.28	33.48	32.10		
V	341.58	327.20	411.20	324.00	290.60	271.40	206.80	199.96	225.60	170.94	169.12	133.22
Cr	170.17	156.06	29.62	75.00	321.40	259.60	374.40	531.20	2084.00	1279.20	1736.60	1521.00
Co	46.42	40.48	32.28	33.62	47.38	42.90	50.22	47.14	106.26	75.42	90.22	82.80
Ni	90.85	84.34	24.36	26.76	69.80	57.66	200.00	318.40	969.60	942.40	765.20	676.40
Rb	0.93	1.80	8.77	28.08	4.41	15.97	18.30	11.99	0.39	2.65	0.33	0.35
Sr	165.77	90.60	239.80	83.92	595.80	912.40	504.60	489.20	19.14	80.32	23.78	26.28
Y	22.13	20.96	48.56	26.64	23.86	21.78	19.06	18.68	13.38	13.73	14.20	9.93
Zr	64.05	58.12	244.60	142.85	98.00	99.71	164.27	165.81	72.57	61.40	75.46	49.68
Nb	5.21	4.74	19.80	16.34	10.42	12.05	36.92	36.86	11.93	8.00	11.63	7.66
Ba	61.60	108.60	143.00	171.16	84.16	573.00	245.20	223.20	4.93	37.10	7.82	5.36
La	4.29	4.03	18.02	14.00	9.53	10.22	27.92	27.24	7.39	11.07	7.11	5.27
Ce	10.71	10.18	45.82	31.00	24.26	25.42	58.06	54.82	17.65	21.72	19.02	13.76
Pr	1.63	1.55	6.41	4.12	3.33	3.35	7.24	6.87	2.36	2.63	2.62	1.88
Nd	8.17	7.77	28.16	17.81	15.17	14.85	29.98	28.22	10.46	10.52	11.62	8.28
Sm	2.55	2.41	7.62	4.44	4.31	4.00	6.30	5.95	2.66	2.33	3.03	2.09
Eu	0.99	0.84	2.60	1.40	1.58	1.54	2.02	1.95	0.96	0.71	0.97	0.80
Gd	3.40	3.21	8.95	4.68	5.02	4.61	5.87	5.63	2.77	2.32	3.28	2.32
Tb	0.58	0.55	1.53	0.74	0.78	0.71	0.78	0.75	0.42	0.36	0.50	0.35
Dy	3.94	3.66	9.47	4.56	4.65	4.27	4.18	4.03	2.46	2.21	2.94	2.07
Ho	0.84	0.79	2.04	0.93	0.89	0.83	0.73	0.72	0.46	0.46	0.56	0.39
Er	2.47	2.33	5.64	2.58	2.36	2.23	1.84	1.82	1.23	1.31	1.46	1.04
Tm	0.35	0.33	0.82	0.36	0.31	0.30	0.23	0.22	0.16	0.19	0.19	0.14
Yb	2.37	2.21	5.06	2.25	1.89	1.81	1.37	1.35	0.94	1.20	1.17	0.84
Lu	0.35	0.32	0.75	0.33	0.26	0.26	0.18	0.18	0.13	0.18	0.16	0.11
Hf	1.61	1.49	5.59	3.10	2.58	2.60	3.93	3.94	1.99	1.51	2.03	1.39
Ta	0.35	0.31	1.26	0.99	0.66	0.77	2.13	2.09	0.77	0.46	0.68	0.45
Pb	1.15	1.93	1.87	2.22	5.36	6.35	3.18	3.38	0.45	3.40	0.45	0.36
Th	0.39	0.35	1.36	1.33	0.83	1.04	2.86	2.78	0.75	2.90	0.75	0.45
U	0.11	0.11	0.55	0.44	0.30	0.29	0.49	0.40	0.16	0.52	0.24	0.16

SAB = subalkaline basalt; AB = alkaline basalt. LJS = Lajishan, YJ = Yongjing.

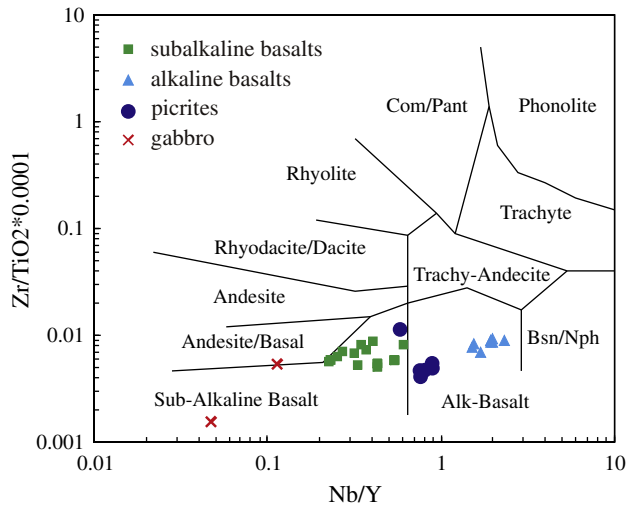


Fig. 4. Nb/Y–Zr/Ti (Winchester and Floyd, 1976) diagrams for basaltic rocks from the Lajishan ophiolites, Qilian Orogen.

tectonic discrimination diagrams, compared with the sub-alkaline basalts (see below).

- (3) Picrites. One sample (13QLS-137) occurs as massive picrite below the pillow lavas layer, and others crop out as pillowed picrites in the field. These rocks are characterised by high MgO (> 18 wt%) with 48–52 wt% SiO₂. Most of samples have higher TiO₂ than 1% except for massive basalt 13QLS-137. The major element composition closely analogous to komatiites (TiO₂ < 1 wt%) and mameichite (TiO₂ > 1 wt%) classified by Le Bas (2000), however, they do not have a spinifex texture and

are termed picrites. In the Nb/Y–Zr/Ti diagram, the pillowed picrites plot in the alkaline field, while the massive picrite plots in the sub-alkaline field. They are also classified as alkaline series with significant negative Sr and Rb, Ba and Sr anomalies. They show similar REE and multi-element patterns to the E-MORB, except for the strong Rb, Ba and Sr depletion (Fig. 5e,f).

4.2.2. Spinel

Chromian spinel (Mg, Fe^{2+})(Cr, Al, Fe^{3+})₂O₄ is a ubiquitous accessory phase in basalts and peridotites, which is effective for distinguishing tectonic settings and the degree of mantle partial melting (Dick and Bullen, 1984). Chromian-rich spinels have been observed in three rock-types in the study area, including cumulate pyroxenite, alkaline basalts and picrites in the LYO (Appendix Table 2). As shown in Fig. 7a, chromian spinels from the cumulate pyroxenite show a wide range of TiO₂ between 0.11–1.08 wt% (mostly > 0.5 wt%), and a narrow range of Al₂O₃. Their Cr[#] (Cr/(Cr + Al)) values are 0.55–0.70, higher than that of the N-type MORB and abyssal peridotite (Fig. 7b, mostly < 0.6) (e.g., Dick and Bullen, 1984). Spinel from the alkaline basalts (12LJ-32) have high TiO₂ and Al₂O₃, but low Cr[#]. Spinel from the picrites (13QLS-115, 116) have high content of TiO₂ (1.60–2.88 wt%) but relatively low Al₂O₃, and mostly plot in the field of OIB (Fig. 7a). They also have high Cr[#] (Cr[#] = Cr/(Cr + Al)), ranging from 0.52 to 0.64 (Appendix Table 2), higher than spinels from the Ontong Java Plateau (0.46–0.52, Sano, 2015).

The spinel composition, as indicated by numerous studies, is a complex function of magma and source peridotite compositions (Kamenetsky et al., 2001). Magmatic abundances of trivalent (Al, Cr) and tetravalent (Ti) cations, unlike Mg²⁺ and Fe²⁺ in spinel, experience very little change during post-entrapment re-equilibration because of their low diffusivity, so they can be used to infer magmatic source

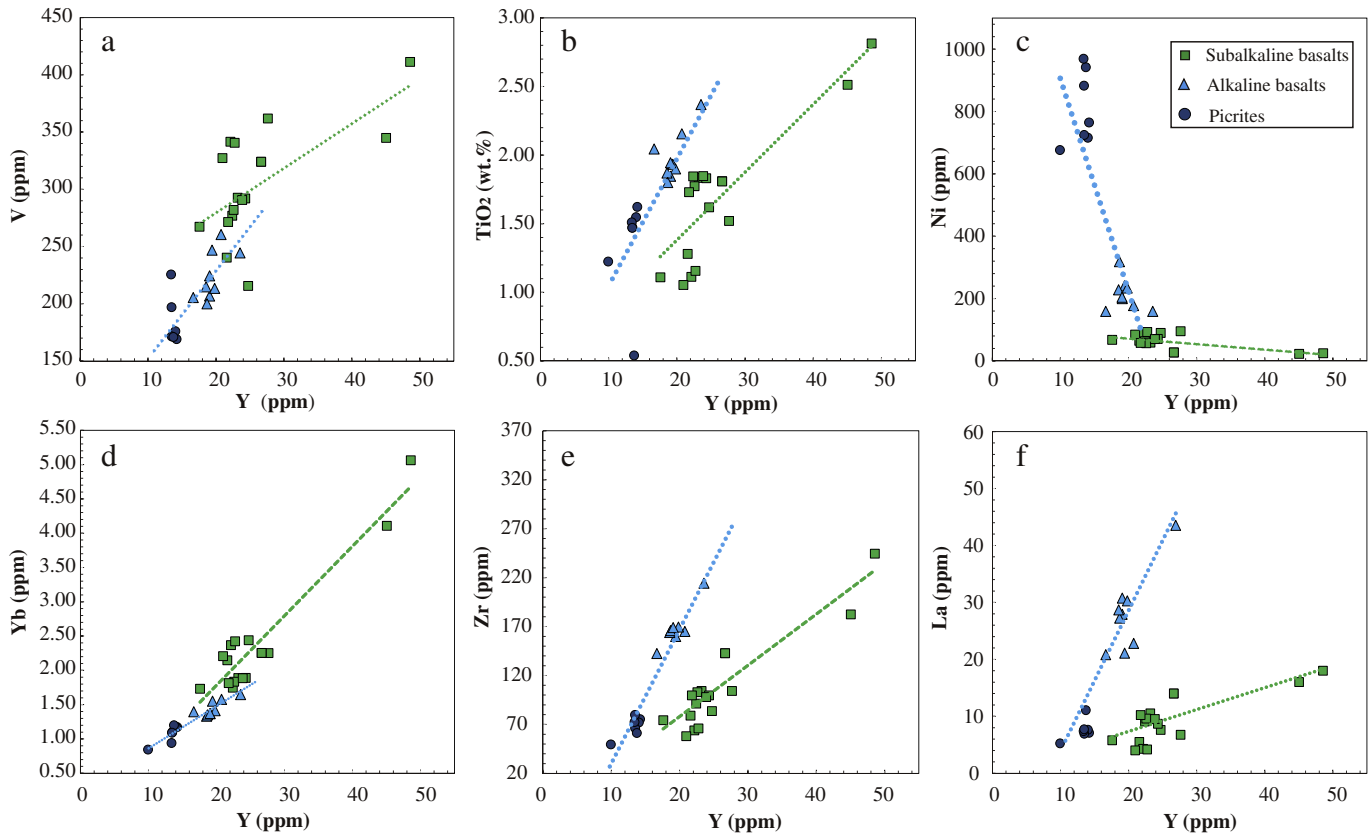


Fig. 5. Variation of selected major and trace elements vs. Y for volcanic rocks from the Lajishan ophiolite, along with regression lines of different groups of basalts (subalkaline and alkaline series). Major element oxides are recalculated on anhydrous bases.

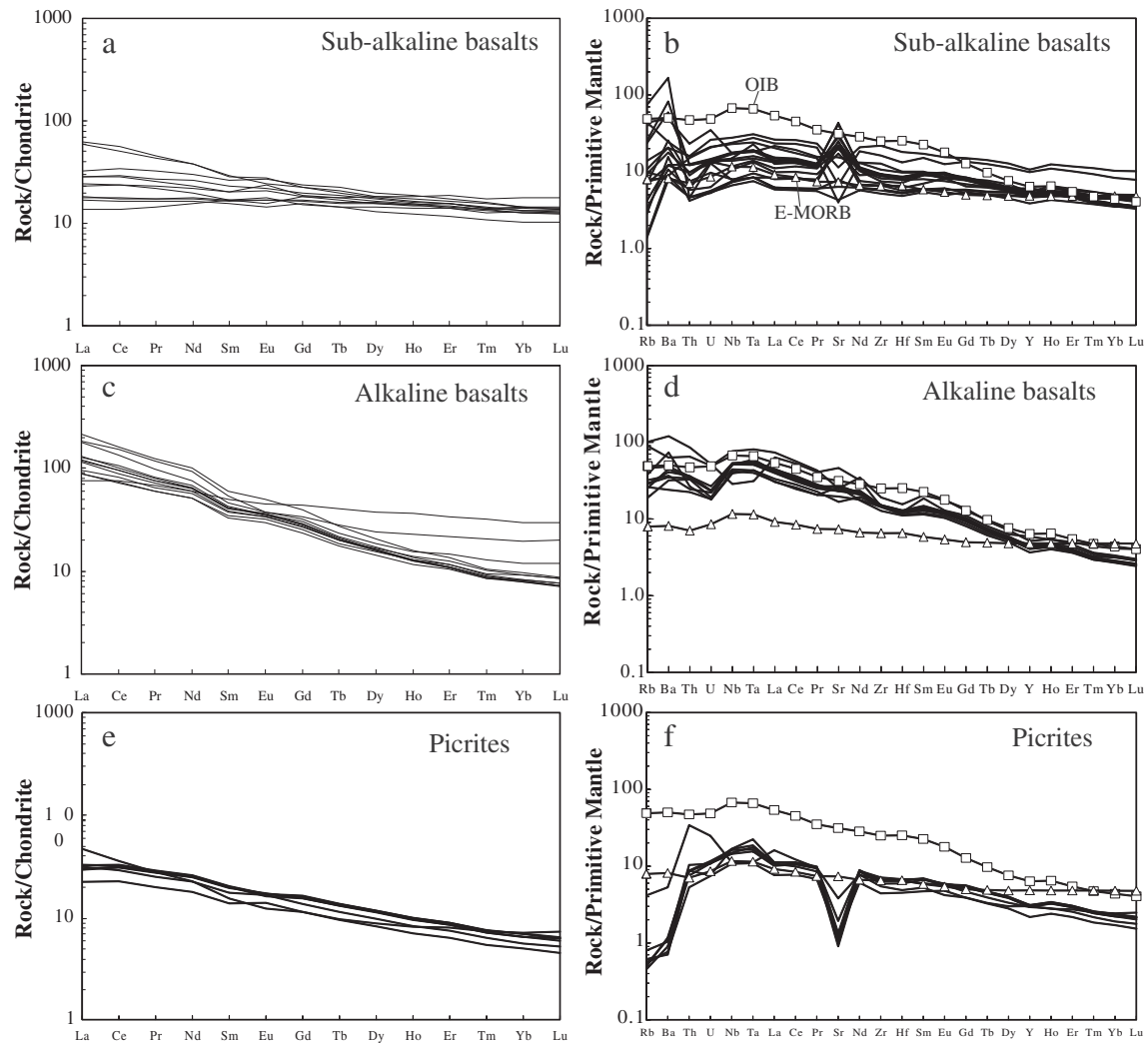


Fig. 6. Chondrite-normalised REE patterns (a, c, e) and primitive mantle normalised trace element patterns (b, d, f) for three groups of samples respectively. Also shown are compositions of OIB in (d) and (f) and enriched MORB (E-type MORB) in (b) for comparison. The normalisation values and the OIB and E-type MORB values are from Sun and McDonough (1989).

(Barnes, 1998; Kamenetsky et al., 2001; Roeder and Campbell, 1985). A positive correlation between Al_2O_3 and TiO_2 in spinel and coexisting melt is demonstrated over significant intervals of averaged spinel and melt compositions sampled from a variety of magmatic types and tectonic environments (Crawford, 1980; Dick and Bullen, 1984; Kamenetsky, 1996). The dependence of spinel Al_2O_3 and TiO_2 concentrations on the parental melt composition suggests the use of an Al_2O_3 vs. TiO_2 diagram to discriminate spinel that crystallised from different magmas in different tectonic environments (Kamenetsky et al., 2001). The relationships between Al_2O_3 and TiO_2 (Fig. 7a) of the alkaline and picrites show relatively high TiO_2 . As shown in Fig. 7b, the picrites and pyroxenite possess higher $\text{Cr}^\#$ than normal MORB and abyssal peridotite. The compositions of different spinels are also plotted in the $\text{Cr}-\text{Al}-\text{Fe}^{3+}$ ternary diagram (Fig. 7c), where picrites plot in the oceanic LIP (OLIP) field while alkaline basalts possess relatively lower Cr compositions.

4.2.3. Whole-rock Sr–Nd isotopic data

Oceanic island basalts have gained a lot of attention because their isotopic compositions are different from MORB, reflecting different mantle source regions (Hofmann and Hart, 1978). Six sub-alkaline, three alkaline basalts and two picrites were analyzed for whole-rock Sr–Nd isotopic composition. The results are presented in Table 2 and illustrated in Fig. 8. The initial values of the Sr–Nd isotope were calculated at 525 Ma. The sub-alkaline and alkaline basalts have variable $^{87}\text{Sr}/^{86}\text{Sr}$

ratios. The sub-alkaline basalts possess relatively higher $^{143}\text{Nd}/^{144}\text{Nd}$ values than alkaline basalts. Most of the basalts have positive $\varepsilon_{\text{Nd}}(T)$ values (0.9–8.9) except for sample 12LJ-29 which have negative $\varepsilon_{\text{Nd}}(T)$ of -0.1 . The positive $\varepsilon_{\text{Nd}}(T)$ values are similar to those of modern plume-related OIB (White and Duncan, 1996; Zindler, 1986). The relatively high initial Sr isotopic values in some samples may be attributed to the alteration by sea water and hydrothermal fluids.

4.3. U–Pb zircon age

One gabbro sample (LJ-26) that occurs as a sill within the pillow lavas was selected for LA-ICP-MS zircon U–Pb dating. The result is given in Appendix Table 3 and illustrated in Fig. 9. About 45 zircon grains were recovered and they are colourless, euhedral to irregular crystals with varying long axis (50–250 μm and length/width ratios of 1.2–2.5). CL images show dark to intermediate luminescence with straight and wide oscillatory growth bands (Appendix Fig. 1a,b).

Zircons from the sample have relatively high Th/U (0.34–1.56). Nineteen spots were analysed on nineteen zircon grains, yielding apparent $^{206}\text{Pb}/^{238}\text{U}$ ages of 507–531 Ma, and forming a concordia age of 525 ± 3 Ma (mean square weighted deviation, MSWD = 0.52) (Appendix Fig. 1c). This age would, at least, represent the minimum formation age of the ophiolite, within the time span of the Qilian Ocean (ca. 550–500 Ma, Song et al., 2013).

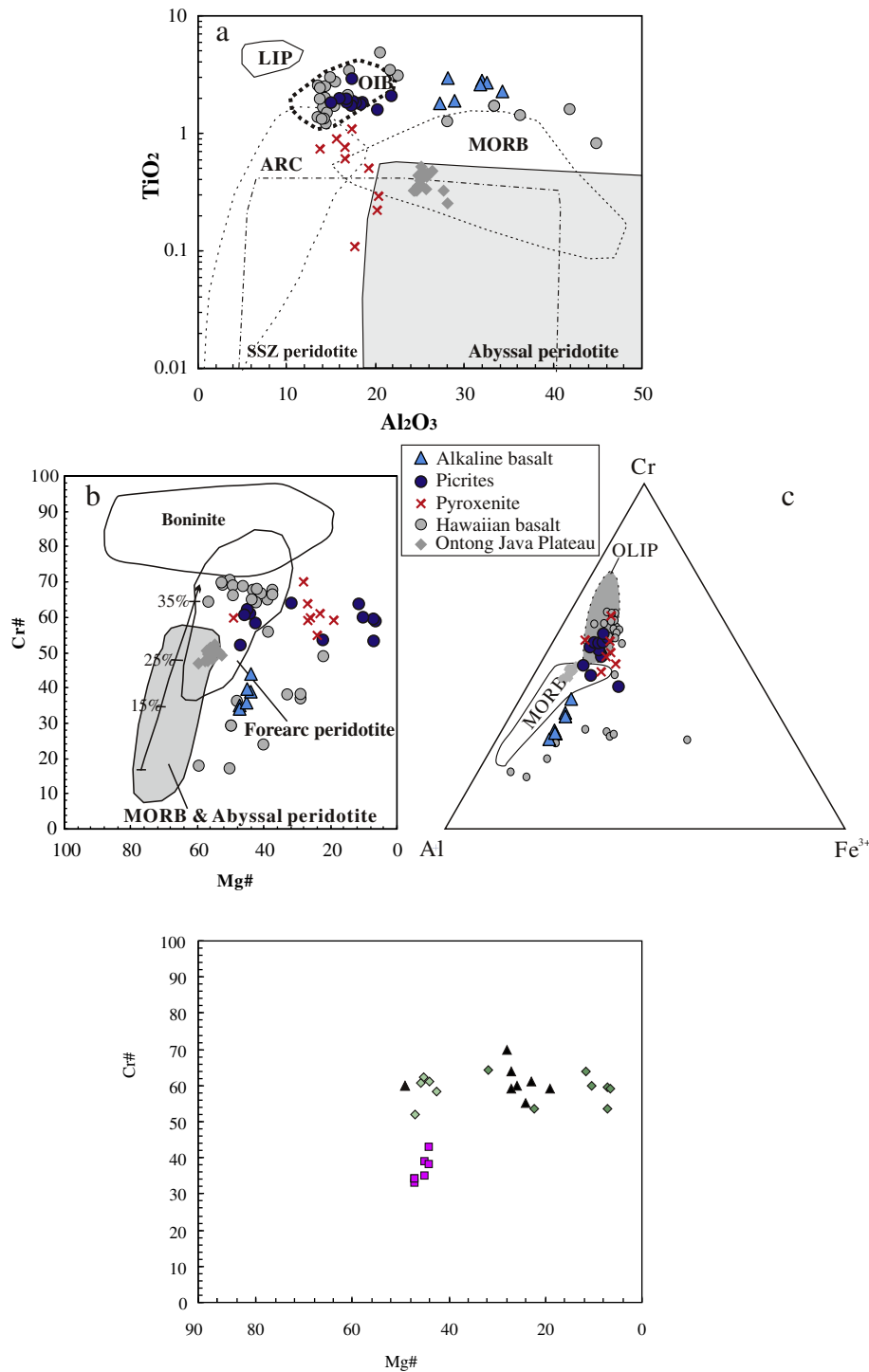


Fig. 7. Spinel compositions of the Lajishan-Yongjing ophiolites. (a) Al_2O_3 vs TiO_2 diagram for spinels from alkaline, picrites and pyroxenites (Kamenetsky et al., 2001) (b) $\text{Cr}^\#$ [Cr/(Cr + Al)] vs $\text{Mg}^\#$ [Mg/(Mg + Fe²⁺)] diagram for spinels (Dick and Bullen, 1984). (c) Cr-Al-Fe³⁺ ternary plot for chromian spinel. Discrimination fields of oceanic large igneous province (OLIP) are from Tokuyama and Batiza (1981); MORB are from Gaetani et al. (1995). Spinel data of the Ontong Java Plateau and Hawaiian basalts are from Sano (2015) and Norman and Garcia (1999), respectively.

5. Discussion

5.1. Petrogenesis and forming conditions

5.1.1. Effect of subsequent alteration

Influences on the major element contents can be measured by CIA value [$\text{Al}_2\text{O}_3/(\text{Al}_2\text{O}_3 + \text{CaO} + \text{Na}_2\text{O} + \text{K}_2\text{O})$] in molecular proportions (Nesbitt and Young, 1982). The CIA values of the LYO basalts range from 28% to 53% and most of them are in a limited range of 30%–49%

(Table 1 and Appendix Table 1), consistent with the CIA values of fresh basalts (CIA = 30–45%, Nesbitt and Young, 1982). It implies no significant changes of the major elements of the three basalt groups. Some mobile elements like Na, K and Al are active elements, and can be changed easily during alteration, which are readily shown in correlations between Zr with Na_2O , K_2O and Al_2O_3 (Hacker et al., 1992). However, Mg is generally an inactive element and its content is not significantly changed during alteration. MgO content in our samples is consistent with the high contents of Cr and Ni. So we think the high

Table 2
Whole-rock Sr–Nd isotopic data for basalts from Lajishan–Yongjing ophiolites.

	Rb (ppm)	Sr (ppm)	⁸⁷ Rb/ ⁸⁶ Sr	⁸⁷ Sr/ ⁸⁶ Sr	I _{Sr} (t)	Sm (ppm)	Nd (ppm)	¹⁴⁷ Sm/ ¹⁴⁴ Nd	¹⁴³ Nd/ ¹⁴⁴ Nd	εNd (T)
<i>Subalkaline basalts</i>										
12LJ-19	0.93	165.8	0.0158	0.705552	0.70543	2.55	8.17	0.1977	0.512815	3.4
12LJ-20	1.8	90.6	0.056	0.705374	0.70495	2.41	7.77	0.197	0.512861	4.3
13QLS-78	6.81	453.8	0.0424	0.705613	0.7053	2.61	9.2	0.1802	0.513021	8.6
13QLS-96	27.88	325.8	0.2417	0.708084	0.70628	4.32	17.63	0.1555	0.512916	8.2
13QLS-105	1.5	437.8	0.0097	0.707115	0.70704	3.08	10.87	0.1801	0.513034	8.9
13QLS-111	6.18	419.6	0.0416	0.704649	0.70434	4.01	13.86	0.1834	0.512996	7.9
<i>Alkaline basalts</i>										
12LJ-28	18.3	504.6	0.1024	0.705622	0.70486	6.3	29.98	0.1334	0.512466	0.9
12LJ-29	11.99	489.2	0.0693	0.705543	0.70502	5.95	28.22	0.1338	0.512418	−0.1
12LJ-36	16.07	576.6	0.0787	0.706013	0.70542	6.14	29.24	0.1332	0.512505	1.7
<i>Picrites</i>										
13QLS-115	0.39	19.14	0.0578	0.703854	0.70342	2.66	10.46	0.1612	0.512787	5.3
13QLS-116	0.51	40.94	0.035	0.706623	0.70636	3.02	11.78	0.1628	0.512795	5.4

Note
(1) $I_{Sr} = \frac{{}^{87}Sr/{}^{86}Sr - {}^{87}Rb/{}^{86}Sr \times (e^{\lambda_{Rb}T} - 1)}{{}^{87}Sr/{}^{86}Sr - {}^{87}Rb/{}^{86}Sr \times (e^{\lambda_{Rb}T} - 1)}$, where $\lambda_{Rb} = 1.42 \times 10^{-11} \text{ year}^{-1}$.
(2) $\epsilon_{Nd}(T) = \left\{ \frac{[{}^{143}Nd/{}^{144}Nd] - [{}^{143}Nd/{}^{144}Nd]_{CHUR(0)}}{[{}^{143}Nd/{}^{144}Nd]_{CHUR(0)}} - 1 \right\} \times 10,000$, where $\lambda_{Sm} = 6.54 \times 10^{-12} \text{ year}^{-1}$; $[{}^{143}Nd/{}^{144}Nd]_{CHUR(0)} = 0.512638$; $[{}^{147}Sm/{}^{144}Nd]_{CHUR(0)} = 0.1967$.
(3) $T = 525 \text{ Ma}$, crystallisation age of the Lajishan–Yongjing basalt.

MgO composition is a primitive geochemical feature, rather than a result of subsequent alteration.

The mobility of trace elements can be evaluated by plotting Zr against other trace elements, such as the rare earth elements (La, Yb, Sr), HFSE (Th, Nb, Ti and Ta), Y and U, in covariance diagrams (Cann, 1970; Li et al., 2008, 2010). As shown in Fig. 9, the trace elements possess a linear relationship with Zr, which indicates that the trace elements are immobile during later ocean floor alteration and metamorphism. The following petrological interpretations will be based on analysis of these immobile elements.

5.1.2. Crustal contamination and fractional crystallisation

The trace element patterns resemble those of OIB, including the positive Nb and Ta anomalies. The highly variable ${}^{87}Sr/{}^{86}Sr$ ratios (0.703854–0.708084) suggested a hydrothermal alteration, but $\epsilon_{Nd}(T)$ values (0.9–8.9) are similar to present-day OIB, indicating no significant contamination by continental crust. The incompatible elemental ratios such as $Zr/Nb = 3.92$ – 14.26 , $Ba/Nb = 0.41$ – 27.62 in the studied basalts are lower than those of continental crust ($Zr/Nb = 16.2$, $Ba/Nb = 54$; Hofmann et al., 1986), which indicate that they lack

continental lithospheric sources. We conclude that they formed in an oceanic lithosphere setting.

The large variation in MgO (3.97–22.40) and $Mg^\#$ (44.47–78.42) of the three types of basalt implicates processes of fractional crystallisation. In the correlation diagrams between Ni, V and Cr (Fig. 10), the primary magmas for the sub-alkaline and alkaline basalts might have experienced varying degrees of clinopyroxene-dominated (with olivine) fractionation.

Ni is a compatible element in olivine, so the Ni contents would have a high level if the basalts have accumulated olivines. As shown in Fig. 10, the LYO picrites possess similar composition of Ni contents in comparison with Hawaiian picrites and representative komatiites (Fig. 10). Therefore, it also provides evidence that these picrites have not experienced olivine accumulation. As the incompatible trace element concentrations and patterns are consistent with melt, not cumulate, values (Fig. 6e, f), we consider that the picrites most likely represent primary or near-primary magma compositions.

5.1.3. Mantle conditions

Mantle source temperature represents the temperature of mantle material if it adiabatically ascended to the Earth's surface without melting (McKenzie and Bickle, 1988). Highly magnesian volcanic rocks are widely used to estimate mantle melting conditions and mantle compositions because their compositions are thought to be close to the primary mantle-derived melts (Larsen and Pedersen, 2000).

We use the PRIMELT3 software to calculate T_p for mantle, in order to distinguish relatively hotter from colder mantle sources, which is important in understanding the thermal characteristics of ambient and anomalous mantle (Herzberg and Asimow, 2015). We choose the picrites which have the closest affinity with primary magma, and regard the geochemistry of these picrites as representative of primary magma compositions. The results of primary melt composition, T_p and degree of partial melting (F) calculations are listed in Appendix Table 4. Using parameterised experimental data on mantle melting phase relations, we estimated that the T_p is 1489–1600 °C (the potential temperature of the mantle source is obtained in terms of the equation of:

$$T_p (\text{°C}) = 1025 + 28.6MgO - 0.084 * MgO^2,$$

Herzberg et al., 2007). The T_p is obviously higher than the 1350 °C of the upper mantle (Davies, 2009; Korenaga, 2008), and close to the 1500–1600 °C of Hawaiian picrites (Herzberg et al., 2007; Lee et al., 2009), which demonstrates an anomalously hot mantle source for the Cambrian volcanics.

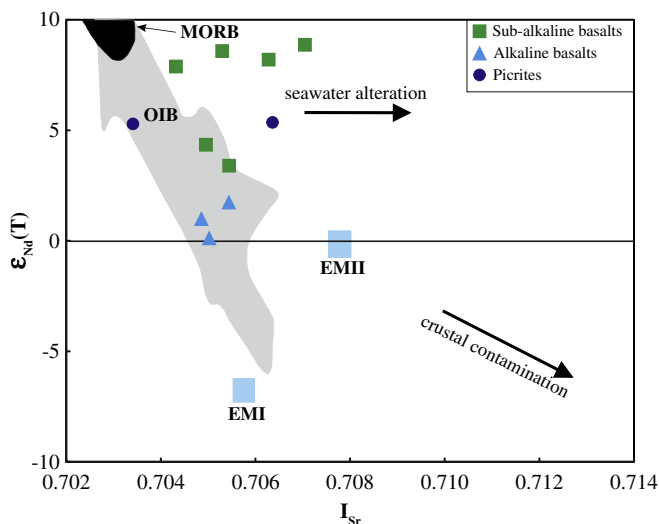


Fig. 8. Sr–Nd isotopic compositions for the Lajishan basalts. Plotted for comparison are: the modern depleted upper mantle (N-MORB) (Zimmer et al., 1995), OIB (White and Duncan, 1996; Zindler, 1986), and EMI and EMII member (Hart, 1988).

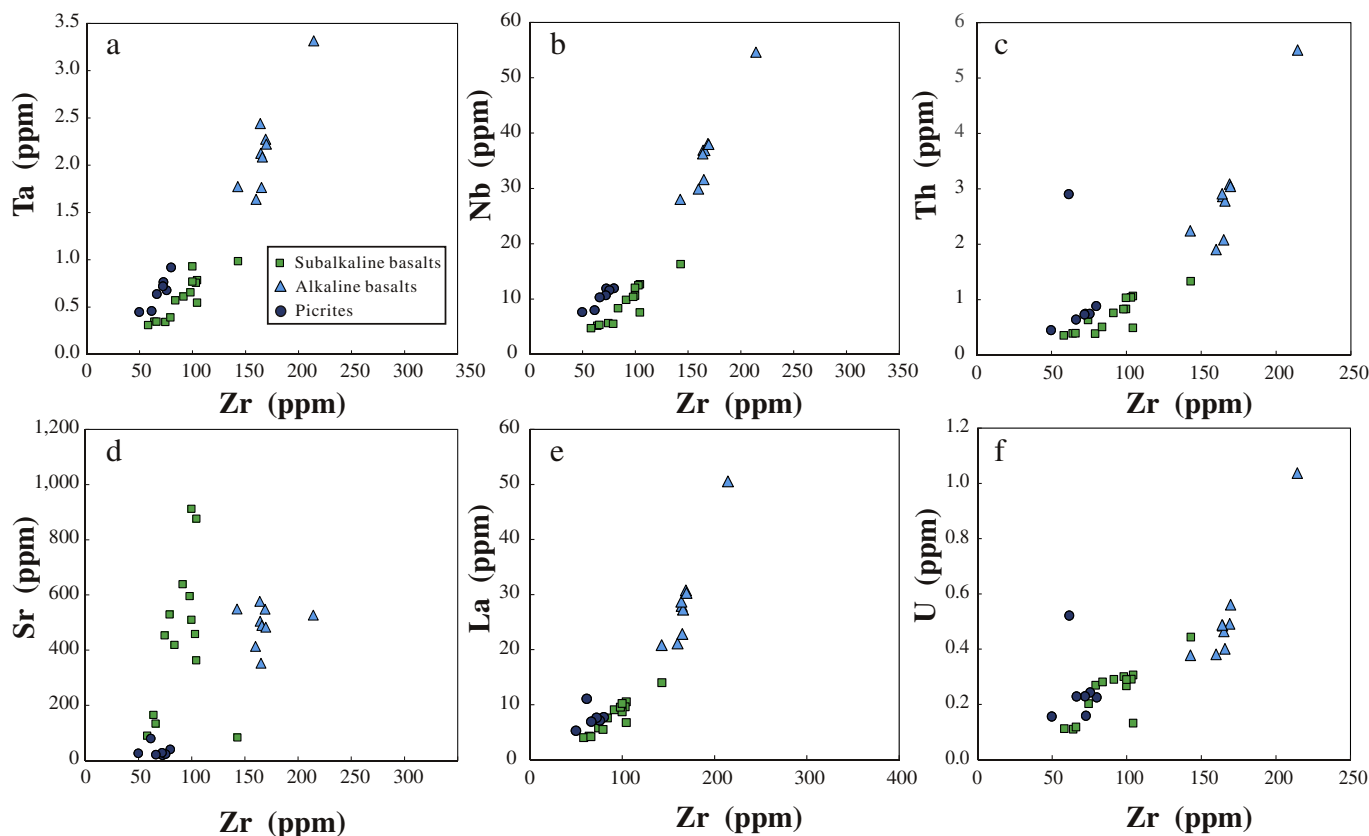


Fig. 9. Correlation diagrams of zirconium versus selected trace elements to measure their mobilities. Most of the elements have a linear relationship with Zr except for Sr, suggesting that the trace elements are immobile during subsequent alteration. The different linear trends of the three groups are attributed to their variable mantle sources (also see Fig. 5).

5.1.4. Degree of partial melting

Cr is a compatible element, preferring to stay in residue; only when the degree of melting is high enough does it go into the melt. So the higher the Cr contents are in the melt, the higher degree of melting there is. It is generally thought that spinels in basalts are in equilibrium with melt, and the chromium number ($Cr^\#$) in spinel as an indicator of partial melting correlates well with trace elements (e.g. Dy, Er, Yb) in clinopyroxene. Hellebrand et al. (2001) gave an equation: $F =$

$10\ln(Cr^\#) + 24$ for spinels to estimate the relationship between $Cr^\#$ and F , where F is the degree of melting.

As shown in Appendix Table 2, the calculated F of alkaline basalts ranges from 12.9% to 15.6%; while the F of the picrites ranges from 17.5% to 19.6% and pyroxenites ranges from 18.0% to 20.4%. The calculated F of the picrites using the PRIMELTS 3.0 ranges from 38 to 44%. All the results are higher than of most N-type MORB (~15% by Niu, 1997 or ~6% by Workman and Hart, 2005).

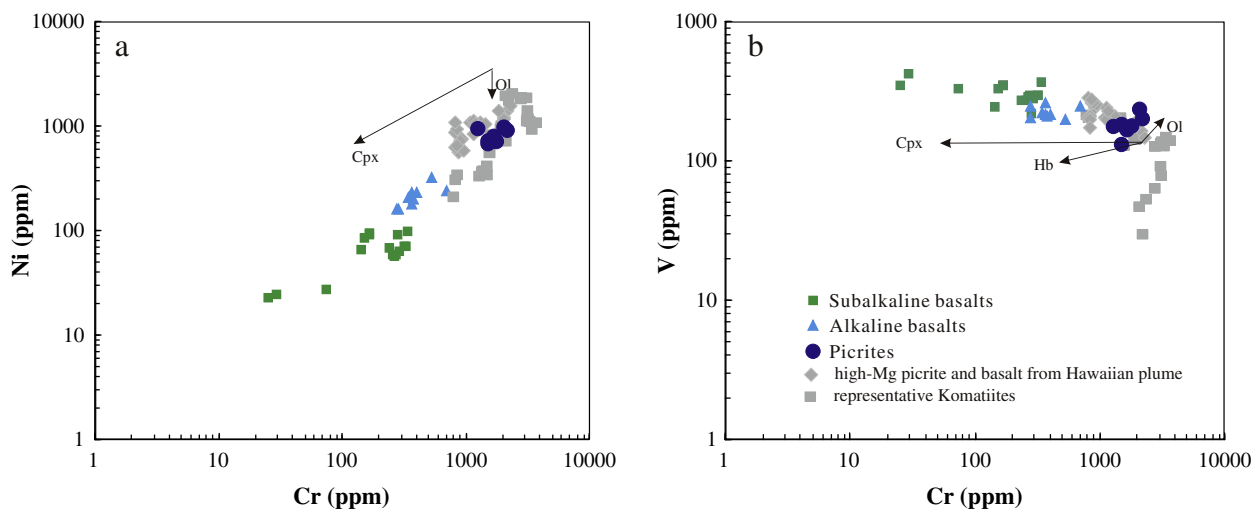


Fig. 10. (a) Ni and (b) V vs. Cr diagrams showing the clinopyroxene-dominated fractionation for alkaline and sub-alkaline basalts and olivine-controlled fractionation for picrites. The vectors are from Li et al. (2010). The compositions of high-Mg picrite and basalts from Hawaii (Norman and Garcia, 1999) and representative komatiites (Puchtel et al., 2016; Van Acken et al., 2016) are also shown in the figures for comparison.

5.2. Determination of a Cambrian (~525 Ma) oceanic plateau

The basalts in the LYO complexes possess massive and pillow structures associated with abyssal deposits (e.g. red chert), indicating that the eruption was in an underwater environment. All the three rock groups, including sub-alkaline, alkaline and picrites, exhibit E-MORB and OIB-type geochemical features (Fig. 5), which are different from the N-type MORB in most present day ocean ridges. Such a signature is thought to be diagnostic of hot spot or plume related basalts associated with oceanic islands (Hofmann, 1997).

In the Th/Yb vs. Ta/Yb diagram (Fig. 11a), the sub-alkaline basalts are close to the E-MORB composition, the alkaline basalts close to OIB composition; and the picrites plot between OIB and E-MORB compositions (Sun and McDonough, 1989). In the Nb/Y and Zr/Y variation diagrams (Fig. 11b), all samples plot within the field of Icelandic data (Fitton et al., 1997).

Ratios of highly incompatible trace elements in basalts reflect the geochemical composition of their mantle sources and therefore provide information about the distribution of the HFSE in the mantle. As shown in Fig. 11c, Nb/Ta ratios in OIB are decoupled from Zr/Hf ratios (Pfänder et al., 2007). Moreover, most of the samples are plotted in the same field as OIBs from the world's main oceanic plateaus like Rurutu (Chauvel et al., 1997), Tubuai (Chauvel et al., 1992), Azores (Bieier et al., 2006), Pitcairn (Eisele et al., 2002) and Samoa (Workman et al., 2004), which

are shown in the field of OIB in Fig. 11c. In the Nb/La vs Nb/Th diagram (Fig. 11d), picrites are quite similar to the Kostomuksha komatiites except for higher Nb contents, and most of the picrites lie close to the field of recent oceanic plateaus.

The REE compositions of basalts from the LYO show marked LREE/MREE enrichment ($La_N/Sm_N = 1.04–3.17$) coupled with prominent MREE/HREE enrichment ($Sm_N/Yb_N = 1.19–5.19$). Besides, all the samples possess low contents of HREE with right inclined patterns (Fig. 5), suggesting that these basalts were derived from the source region with the presence of garnet as a residual phase that preferentially holds heavy REEs (Irving and Frey, 1978). Using the Fractionate-PT model of Lee et al. (2009), the calculated depths of melting range from 2.0–3.4 GPa (Table 3), in accordance with depths where garnet is a residual phase.

In summary, on the basis of petrology, geochemical and isotopic data described above, we conclude that the basalts form LYO complexes formed in an intra-oceanic setting, most likely an oceanic plateau associated with a mantle plume: no other explanation seems viable due to the presence of the picrites.

5.3. Tectonic implications: trench jam and new intra-oceanic arc generation

When a subducting ocean plate contains a body that is too buoyant to subduct the phenomenon of “trench jam” can occur (e.g., Abbott et al., 1997; Niu et al., 2003, 2015), with the consequence that a new

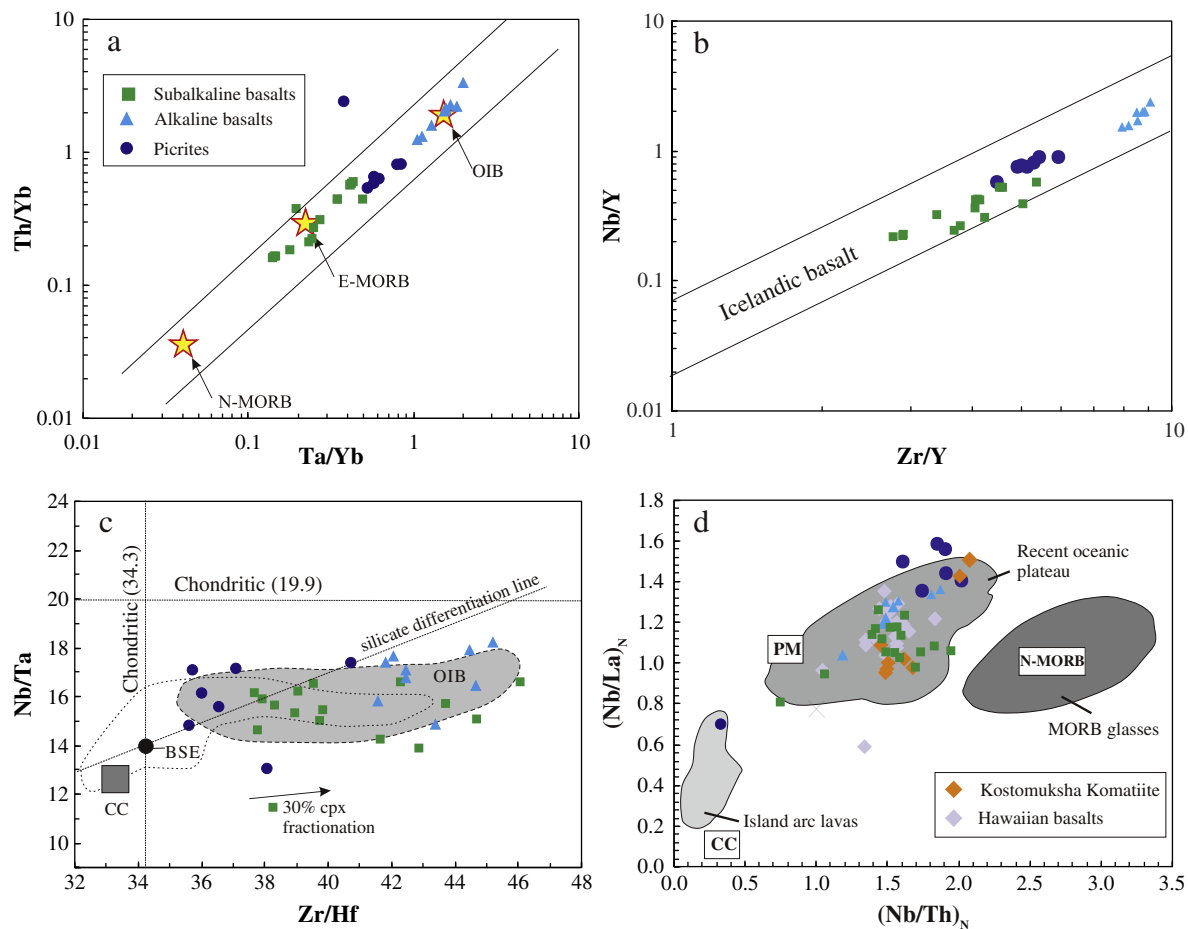


Fig. 11. Tectonic discrimination diagrams for various rock series the Lajishan–Yongjiing ophiolitic complexes (a) Ta/Yb vs. Th/Yb diagram for basalts from the Lajishan ophiolitic complex (modified after Pearce, 1982). The compositions of modern normal mid-ocean ridge basalt (N-MORB), enriched mid-ocean ridge basalt (E-MORB), and ocean-island basalt (OIB) are from Sun and McDonough (1989); (b) Nb/Y-Zr/Y diagram from Fitton et al. (1997); (c) Nb/Ta versus Zr/Hf in ocean island basalts. Also shown is the field for MORB, average composition of the continental crust (CC, Zr/Hf and Nb/Ta from Barth et al., 2000) and OIB from Pfänder et al. (2007), Bieier et al. (2006), Chauvel et al. (1992), Chauvel et al. (1997), Eisele et al. (2002), Münker et al. (2003). Chondritic Nb/Ta and Zr/Hf from Münker et al. (2003). The arrow indicates the shift in Zr/Hf and Nb/Ta that results from 30% clinopyroxene fractionation (calculated from Pfänder et al., 2007). (d) Primitive mantle-normalised (Nb/Th)_N vs. (Nb/La)_N data for LYO picrites and basalts. Normalisation values are from Sun and McDonough (1989). Data from Kostomuksha komatiite (Puchtel et al., 1998) and Hawaiian basalts (Norman and Garcia, 1999) are added for comparison. The field of recent oceanic plateau, MORB and island arc tholeiites are from Puchtel et al. (1998).

Table 3

Results of depths of partial melting of picrites calculated by using FractionatePT of Lee et al. (2009).

Sample	Thermobarometric results							
	T Putirka 2005 NaK model C	P Lee	P Albarede	T Putirka 2005 no comp model A	P Lee	P Albarede	T Lee (no P dependence)	P Lee (with T Lee)
	Celsius	GPa	GPa	Celsius	GPa	GPa	T °C	GPa
13QLS-115	1564.6	3.0	2.9	1652.1	3.5	3.6	1533.9	2.9
13QLS-116	1486.5	2.3	2.2	1617.9	2.8	3.1	1395.1	2.0
LJ15-174	1535.4	3.5	3.5	1674.1	4.3	4.9	1519.5	3.4
LJ15-175	1519.3	2.7	2.5	1642.4	3.2	3.5	1453.7	2.4
LJ15-176	1516.4	2.9	2.9	1637.4	3.5	3.9	1476.3	2.7
LJ15-178	1550.3	3.6	3.6	1688.5	4.4	5.0	1523.9	3.4

subduction zone and volcanic arc are generated. Oceanic plateaus are the best candidates for such a buoyant and unsubductable mass, given the relatively low densities of the high percentage melts present in such crust (Herzberg, 1999; Niu and Batiza, 1991; Niu et al., 2003; O'Hara, 1973).

As described above, the picrites and OIB-type basalts in the LYO are interpreted to be the products of melting of a mantle plume, and they did not experience subduction, but were obducted as an ophiolitic component in the South Qilian Accretionary Belt. The age data (525 ± 3 Ma) reveals that at least a component of the oceanic crust formed in the Late Cambrian. More importantly, the South Qilian Accretionary Belt has also incorporated intra-oceanic arc volcanic rocks (Fig. 1), which formed in a narrow time span from ~470 to 440 Ma (Yang et al., 2002), much younger in age and shorter in duration than the arc volcanism in the North Qilian Accretionary Belt (Song et al., 2013). We suggest that the newly formed arc volcanic sequence would be closely associated with the collision between the plateau and the pre-existing trench at ~470 Ma, on the basis of the age of the oldest arc volcanics in the South Qilian Accretionary Belt. This scenario is illustrated in Fig. 12.

6. Conclusions

- (1) Geochemical, isotopic and geochronological data suggest that the LYO complexes in the south of the Qilian orogenic belt record mantle plume-related activity in the Qilian Ocean during the Cambrian (~525 Ma).
- (2) Basalts of the LYO exhibit trace element and isotopic characteristics of OIB-related or E-MORB-related magmas that can be divided into three groups: E-MORB affinity sub-alkaline basalts (Group 1), OIB-affinity alkaline basalts (Group 2), and picrites (Group 3). The $\text{Cr}^\#$ of spinels in the picrites suggests that the degree of partial melting is 18–21%, which is higher than the accompanying OIB-like lavas. The potential temperature of mantle (T_p) is 1489–1600 °C, suggesting an anomalously hot mantle source and close to that previously interpreted for Hawaiian picrites.
- (3) Attempted subduction of the buoyant oceanic plateau rocks would have accreted oceanic rocks onto the continental margin, which explains the mechanisms for the preservation of the Lajishan–Yongjing Ophiolites.

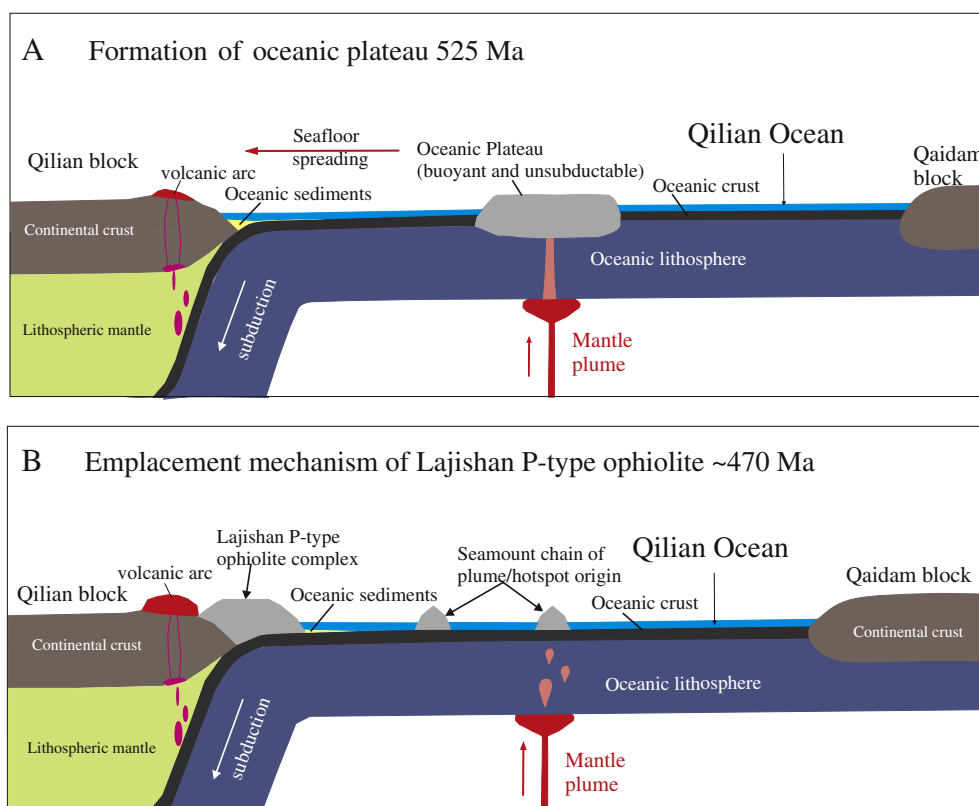


Fig. 12. Cartoons showing the tectono-magmatic evolution for the Lajishan–Yongjing P-type ophiolite complex for the Early Cambrian: (A) plume origin for an oceanic plateau at 525 Ma; (B) The buoyant plateau reached the subduction zone and became a part of newly accreted continent at about 500 Ma. Modified after Niu et al. (2015).

Supplementary data to this article can be found online at <http://dx.doi.org/10.1016/j.lithos.2017.01.027>.

Acknowledgment

We thank Jake Ciborowski, M. L. G. Tejada and Editor-in-chief Andrew Kerr for their constructive official review comments, which led to a better presentation of the final product. This study was supported by National Natural Science Foundation of China (Grant Nos. 41572040), and the Major State Basic Research Development Program (2015CB856105).

References

- Abbott, D.H., Drury, R., Mooney, W.D., 1997. Continents as lithological icebergs: the importance of buoyant lithospheric roots. *Earth and Planetary Science Letters* 149, 15–27.
- Aitken, B.G., Echeverría, L.M., 1984. Petrology and geochemistry of komatiites and tholeiites from Gorgona Island, Colombia. *Contributions to Mineralogy and Petrology* 86, 94–105.
- Arndt, N.T., Kerr, A.C., Tarney, J., 1997. Dynamic melting in plume heads: the formation of Gorgona komatiites and basalts. *Earth and Planetary Science Letters* 146, 289–301.
- Barnes, S.J., 1998. Chromite in Komatiites, 1. Magmatic Controls on Crystallization and Composition. *Journal of Petrology* 39, 1689–1720.
- Barth, M.G., McDonough, W.F., Rudnick, R.L., 2000. Tracking the budget of Nb and Ta in the continental crust. *Chemical Geology* 165, 197–213.
- Bieier, C., Haase, K.M., Hansteen, T.H., 2006. Magma evolution of the Sete Cidades volcano, Sao Miguel, Azores. *Journal of Petrology* 47, 1375–1411.
- Campbell, I.H., Griffiths, R.W., 1990. Implications of mantle plume structure for the evolution of flood basalts. *Earth and Planetary Science Letters* 99, 79–93.
- Cann, J.R., 1970. Rb, Sr, Y, Zr and Nb in some ocean floor basaltic rocks. *Earth and Planetary Science Letters* 10, 7–11.
- Chauvel, C., Hofmann, A.W., Vidal, P., 1992. HIMU-EM: the French-Polynesian connection. *Earth and Planetary Science Letters* 110, 99–119.
- Chauvel, C., McDonough, W.F., Guille, G., Maury, R., Duncan, R., 1997. Contrasting old and young volcanism in Rurutu Island, Austral chain. *Chemical Geology* 139, 125–143.
- Coffin, M.F., Eldholm, O., 1992. Volcanism and continental break-up: a global compilation of large igneous provinces. Geological Society London, Special Publications 68, 17–30.
- Coffin, M.F., Eldholm, O., 1994. Large Igneous Provinces – crustal structure, dimensions, and external consequences. *Reviews of Geophysics* 32, 1–36.
- Condie, K.C., 2001. Mantle Plumes and Their Record in Earth History. Cambridge University Press, Cambridge, pp. 186–194.
- Crawford, A.J., 1980. A clinostatite-bearing cumulate olivine pyroxenite from Howqua, Victoria. *Contributions to Mineralogy and Petrology* 75, 353–367.
- Davies, G.F., 2009. Effect of plate bending on the Urey ratio and the thermal evolution of the mantle. *Earth and Planetary Science Letters* 287, 513–518.
- Dick, H.J.B., Bullen, T., 1984. Chromian spinel as a petrogenetic indicator in abyssal and alpine-type peridotites and spatially associated lavas. *Contributions to Mineralogy and Petrology* 86, 54–76.
- Eisele, J., Sharma, M., Galer, S.J.G., Blichert-Toft, J., Devey, C.W., Hofmann, A.W., 2002. The role of sediment recycling in EM-1 inferred from Os, Pb, Hf, Nd, Sr isotope and trace element systematics of the Pitcairn hotspot. *Earth and Planetary Science Letters* 196, 197–212.
- Fitton, J.G., Saunders, A.D., Norry, M.J., 1997. Thermal and chemical structure of the Iceland plume. *Earth and Planetary Science Letters* 153 (3–4), 197–208.
- Gaetani, G.A., Delong, S.E., Wark, D.A., 1995. Petrogenesis of basalts from the Blanco Trough, northeast Pacific: inferences for off-axis melt generation. *Journal of Geophysical Research-Atmospheres* 100 (B3), 4197–4214.
- Greenough, J.D., Dostal, J., Mallory-Greenough, L.M., 2005. Oceanic island volcanism I: mineralogy and petrology. *Geoscience Canada* 32, 29–45.
- Hacker, B.R., Ernst, W.G., Barton, M.D., 1992. Metamorphism, geochemistry and origin of magneesian volcanic rocks, Klamath Mountains, California. *Journal of Metamorphic Geology* 10, 55–69.
- Hart, S.R., 1988. Heterogeneous mantle domains: signature, genesis and mixing chronologies. *Earth and Planetary Science Letters* 90, 273–296.
- Hellebrand, E., Snow, J.E., Dick, H.J., Hofmann, A.W., 2001. Coupled major and trace elements as indicators of the extent of melting in mid-ocean-ridge peridotites. *Nature* 410, 677–681.
- Herzberg, C., 1999. Phase equilibrium constraints on the formation of cratonic mantle. Mantle petrology: field observations and high pressure experimentation—a tribute to Francis R. (Joe) Boyd. Geological Society Special Publication 6, 241–258.
- Herzberg, C., Asimow, P.D., 2015. PRIMELT3 MEGA.XLSM software for primary magma calculation: peridotite primary magma MgO contents from the liquidus to the solidus. *Geochemistry, Geophysics, Geosystems* 16, 563–578.
- Herzberg, C., Hara, M.O., 2002. Plume-associated ultramafic magmas of Phanerozoic age. *Journal of Petrology* 43, 1857–1883.
- Herzberg, C., Asimow, P.D., Arndt, N., Niu, Y., Leshner, C.M., Fitton, J.G., 2007. Temperatures in ambient mantle and plumes: constraints from basalts, picrites, and komatiites. *Geochemistry, Geophysics, Geosystems* 8, 1074–1086.
- Hofmann, A.W., 1997. Mantle geochemistry: the message from oceanic volcanism. *Nature* 385, 219–229.
- Hofmann, A.W., Hart, S.R., 1978. An assessment of local and regional isotopic equilibrium in the mantle. *Earth and Planetary Science Letters* 38, 44–62.
- Hofmann, A.W., White, W.M., 1982. Mantle plumes from ancient oceanic crust. *Earth and Planetary Science Letters* 57, 421–436.
- Hofmann, A.W., Jochum, K.P., Seufert, M., White, W.M., 1986. Nb and Pb in oceanic basalts: new constraints on mantle evolution. *Earth and Planetary Science Letters* 79, 33–45.
- Irving, A.J., Frey, F.A., 1978. Distribution of trace elements between garnet megacrysts and host volcanic liquids of kimberlitic to rhyolitic composition. *Geochimica et Cosmochimica Acta* 42, 771–787.
- Jiang, C.F., Wang, Z.Q., Li, J.Y., 2000. Opening Closing Tectonics of Central Orogenic Belt. Geological Jen Publishing House, Beijing, pp. 1–154 (in Chinese).
- Kamenetsky, V., 1996. Methodology for the study of melt inclusions in Cr-spinel, and implications for parental melts of MORB from FAMOUS area. *Earth and Planetary Science Letters* 142, 479–486.
- Kamenetsky, V.S., Crawford, A.J., Meffre, S., 2001. Factors controlling chemistry of magmatic spinel: an empirical study of associated olivine, Cr-spinel and melt inclusions from primitive rocks. *Journal of Petrology* 42, 655–671.
- Kerr, A.C., Arndt, N.T., 2001. A note on the IUGS reclassification of the high-Mg and picritic volcanic rocks. *Journal of Petrology* 42, 2169–2171.
- Kerr, A.C., Mahoney, J.J., 2007. Oceanic plateaus: problematic plumes, potential paradigms. *Chemical Geology* 241, 332–353.
- Kerr, A.C., Marriner, G.F., Arndt, N.T., Tarney, J., Nivia, A., Saunders, A.D., Duncan, R.A., 1996a. The petrogenesis of Gorgona komatiites, picrites and basalts: new field, petrographic and geochemical constraints. *Lithos* 37, 245–260.
- Kerr, A.C., Tarney, J., Marriner, G.F., Klaver, G.T., Saunders, A.D., Thirlwall, M.F., 1996b. The geochemistry and petrogenesis of the late-Cretaceous picrites and basalts of Curaçao, Netherlands Antilles: a remnant of an oceanic plateau. *Contributions to Mineralogy and Petrology* 124, 29–43.
- Korenage, J., 2008. Urey ratio and the structure and evolution of Earth's mantle. *Reviews of Geophysics* 46, RG2007.
- Larsen, L.M., Pedersen, A.K., 2000. Processes in high-Mg, high T magmas: evidence from olivine, chromite and glass in Palaeogene picrites from West Greenland. *Journal of Petrology* 41, 1071–1098.
- Le Bas, M.J., 2000. IUGS Reclassification of the High-Mg and Picritic Volcanic Rocks. *Journal of Petrology* 41, 1467–1470.
- Lee, C.T., Luffi, P., Plank, T., Dalton, H., Leeman, W.P., 2009. Constraints on the depths and temperatures of basaltic magma generation on Earth and other terrestrial planets using new thermobarometers for mafic magmas. *Earth and Planetary Science Letters* 279, 20–33.
- Li, Z.X., Bogdanova, S.V., Collins, A.S., 2008. Assembly, configuration, and break-up history of Rodinia: a synthesis. *Precambrian Research* 160, 179–210.
- Li, X.H., Li, W.X., Li, Q.L., Wang, X.C., Liu, Y., Yang, Y.H., 2010. Petrogenesis and tectonic significance of the ~850 Ma Gangbian alkaline complex in South China: evidence from in situ zircon U–Pb dating, Hf–O isotopes and whole-rock geochemistry. *Lithos* 114, 1–15.
- Ludwig, K.R., 2003. User's Manual for Isoplot 3.00: A Geochronological Toolkit for Microsoft Excel. Spec. Publ. vol. 4. Berkeley Geochronology Center, Berkeley, Calif.
- McKenzie, D.P., Bickle, M.J., 1988. The volume and composition of melt generated by extension of the lithosphere. *Journal of Petrology* 29, 625–679.
- Morgan, W.J., 1971. Convection plumes in the lower mantle. *Nature* 230, 42–43.
- Münker, C., Pfänder, J.A., Weyer, S., Büchl, A., Kleine, T., Mezger, K., 2003. Evolution of planetary cores and the Earth–Moon system from Nb/Ta systematics. *Science* 301, 84–87.
- Nesbitt, H.W., Young, G.M., 1982. Early proterozoic climates and plate motions inferred from major element chemistry of lutites. *Nature* 299 (5885), 715–717.
- Niu, Y., 1997. Mantle melting and melt extraction processes beneath ocean ridges: evidence from abyssal peridotites. *Journal of Petrology* 38, 1047–1074.
- Niu, Y., Batiza, R., 1991. An empirical method for calculating melt compositions produced beneath mid-ocean ridges: application for axis and off-axis (seamounts) melting. *Journal of Geophysical Research-Solid Earth* 96, 21753–21777.
- Niu, Y., O'Hara, M.J., Pearce, J.A., 2003. Initiation of subduction zones as a consequence of lateral compositional buoyancy contrast within the lithosphere: a petrological perspective. *Journal of Petrology* 44, 851–866.
- Niu, Y., Liu, Y., Xue, Q., Shao, F., 2015. Exotic origin of the Chinese continental shelf: new insights into the tectonic evolution of the western Pacific and eastern China since the Mesozoic. *Science Bulletin* 60, 1598–1616.
- Norman, M.D., Garcia, M.O., 1999. Primitive magmas and source characteristics of the Hawaiian plume: petrology and geochemistry of shield picrites. *Earth and Planetary Science Letters* 168, 27–44.
- O'Hara, M.J., 1973. Non-plume magmas and dubious mantle plume beneath Iceland. *Nature* 243, 507–509.
- Pearce, J.A., 1982. Trace element characteristics of lavas from destructive plate boundaries. In: Thorpe, R.S. (Ed.), *Andesites*. John Wiley and Sons, New York, pp. 525–548.
- Pfänder, J.A., Münker, C., Stracke, A., Mezger, K., 2007. Nb/Ta and Zr/Hf in ocean island basalts—implications for crust–mantle differentiation and the fate of Niobium. *Earth and Planetary Science Letters* 254, 158–172.
- Puchtel, I.S., Hofmann, A.W., Mezger, K., 1998. Oceanic plateau model for continental crustal growth in the Archaean: a case study from the Kostomuksha greenstone belt, NW Baltic Shield. *Earth and Planetary Science Letters* 155, 57–74.
- Puchtel, I.S., Touboul, M., Blichert-Toft, J., Walker, R.J., Brandon, A.D., Nicklas, R.W., Kulikov, V.S., Samsonov, A.V., 2016. Lithophile and siderophile element systematics of Earth's mantle at the Archean–Proterozoic boundary: evidence from 2.4 Ga komatiites. *Geochimica et Cosmochimica Acta* 180, 227–255.
- Richards, M.A., Duncan, R.A., Courtillot, V.E., 1989. Flood Basalts and Hot-Spot Tracks: Plume Heads and Tails. *Science* 246, 103–107.

- Roeder, P.L., Campbell, I.H., 1985. The effect of postcumulus reactions on compositions of chrome-spinels from the Jimberlana Intrusion. *Journal of Petrology* 26, 763–786.
- Sano, T., 2015. Homogenization of magmas from the Ontong Java Plateau: olivine-spinel compositional evidence. *Special Paper of the Geological Society of America* 511, 221–232.
- Shimizu, K., Komiya, T., Hirose, K., Shimizu, N., Maruyama, S., 2001. Cr-spinel, an excellent micro-container for retaining primitive melts – implications for a hydrous plume origin for komatiites. *Earth and Planetary Science Letters* 189, 177–188.
- Song, S.G., Zhang, L.F., Niu, Y.L., Su, L., Song, B.A., Liu, D.Y., 2006. Evolution from oceanic subduction to continental collision: a case study of the Northern Tibetan Plateau inferred from geochemical and geochronological data. *Journal of Petrology* 47, 435–455.
- Song, S.G., Zhang, L.F., Niu, Y.L., Wie, C.J., Liou, J.G., Shu, G.M., 2007. Eclogite and carpholite-bearing metasedimentary rocks in the North Qilian suture zone, NW China: implications for Early Palaeozoic cold oceanic subduction and water transport into mantle. *Journal of Metamorphic Geology* 25, 547–563.
- Song, S.G., Niu, Y.L., Zhang, L.F., Wei, C.J., Liou, J.G., Su, L., 2009. Tectonic evolution of Early Palaeozoic HP metamorphic rocks in the North Qilian Mountains, NW China: new perspectives. *Journal of Asian Earth Sciences* 35, 334–353.
- Song, S.G., Su, L., Li, X.H., Zhang, G.B., Niu, Y.L., Zhang, L.F., 2010a. Tracing the 850 Ma continental flood basalts from a piece of subducted continental crust in the North Qaidam UHPM belt, NW China. *Precambrian Research* 183, 805–816.
- Song, S.G., Niu, Y.L., Wei, C.J., Ji, J.Q., Su, L., 2010b. Metamorphism, anatexis, zircon ages and tectonic evolution of the Gongshan block in the northern Indochina continent—an eastern extension of the Lhasa Block. *Lithos* 120, 327–346.
- Song, S.G., Su, L., Li, X.H., Niu, Y.L., Zhang, L.F., 2012. Grenville-age orogenesis in the Qaidam-Qilian block: the link between South China and Tarim. *Precambrian Research* 220–221, 9–22.
- Song, S., Niu, Y., Su, L., Xia, X., 2013. Tectonics of the North Qilian orogen, NW China. *Gondwana Research* 23, 1378–1401.
- Song, S., Niu, Y., Su, L., Zhang, C., Zhang, L., 2014. Continental orogenesis from ocean subduction, continent collision/subduction, to orogen collapse, and orogen recycling: the example of the North Qaidam UHPM belt, NW China. *Earth Science Reviews* 129, 59–84.
- Sun, S.S., McDonough, W.F., 1989. Chemical and isotopic systematics of oceanic basalts: implications for mantle composition and processes. *Geological Society, London, Special Publications* 42, 313–345.
- Tokuyama, H., Batiza, R., 1981. Chemical composition of igneous rocks and origin of the sill and pillow-basalt complex of Nauru Basin, southwest Pacific. *Initial Reports of the Deep Sea Drilling Project* 61, 673–687.
- Tung, K.A., Yang, H.J., Yang, H.Y., Liu, D.Y., Zhang, J.X., Wan, Y.S., Tseng, C.Y., 2007. SHRIMP U–Pb geochronology of the zircons from the Precambrian basement of the Qilian Block and its geological significances. *Chinese Science Bulletin* 52, 2687–2701.
- Tung, K.A., Yang, H.Y., Liu, D.Y., Zhang, J.X., Yang, H.J., Shau, Y.H., 2013. The Neoproterozoic granitoids from the Qilian block, NW China: evidence for a link between the Qilian and South China blocks. *Precambrian Research* 235, 163–189.
- Van Acken, D., Hoffmann, J.E., Schorscher, J.H.D., Schulz, T., Heuser, A., Luguët, A., 2016. Formation of high-Al komatiites from the Mesoarchean Quebra Osso Group, Minas Gerais, Brazil: trace elements, HSE systematics and Os isotopic signatures. *Chemical Geology* 422, 108–121.
- Viljoen, M.J., Viljoen, R.P., 1969. The geology and geochemistry of the lower ultramafic unit of the Onverwacht Group and a proposed new class of igneous rock. *Geological Society of South Africa Special Publication* 2, 55–86.
- Wan, Y.S., Xu, Z.Q., Yang, J.S., Zhang, J.X., 2001. Ages and compositions of the Precambrian high-grade basement of the Qilian terrane and its adjacent areas. *Acta Geologica Sinica-English* 75, 375–384.
- White, W.M., Duncan, R.A., 1996. Geochemistry and geochronology of the Society Islands: new evidence for deep mantle recycling. *Geophysical Monograph Series* 95, 183–206.
- Winchester, J.A., Floyd, P.A., 1976. Geochemical magma type discrimination: application to altered and metamorphosed basic igneous rocks. *Earth and Planetary Science Letters* 28, 459–469.
- Workman, R.K., Hart, S.R., 2005. Major and trace element composition of the depleted MORB mantle (DMM). *Earth and Planetary Science Letters* 231, 53–72.
- Workman, R.K., Hart, S.R., Jackson, M., Regelous, M., Farley, K.A., Blusztajn, J., 2004. Recycled metasomatized lithosphere as the origin of the enriched mantle II (EM2) end-member: evidence from the Samoan volcanic chain. *Geochemistry, Geophysics, Geosystems* 5, 449.
- Wu, H.Q., Feng, Y.M., Song, S.G., 1993. Metamorphism and deformation of blueschist belts and their tectonic implications, north Qilian Mountains, China. *Journal of Metamorphic Geology* 11, 523–536.
- Xiao, W.J., Windley, B.F., Yong, Y., Yan, Z., Yuan, C., Liu, C.Z., Li, J.L., 2009. Early Paleozoic to Devonian multiple-1060 accretionary model for the Qilian Shan, NW China. *Journal of Asian Earth Sciences* 35, 323–333.
- Yang, W., Deng, Q., Xiuling, W.U., 2002. Major characteristics of the Lajishan Orogenic Belt of the South Qilian Mountains and its geotectonic attribute. *Acta Geologica Sinica* 76, 110–117.
- Yin, A., Manning, C.E., Lovera, O., Menold, C.A., Chen, X.H., Gehrels, G.E., 2007. Early Paleozoic tectonic and thermomechanical evolution of ultrahigh-pressure (UHP) metamorphic rocks in the Northern Tibetan Plateau, Northwest China. *International Geology Review* 49, 681–716.
- Zhang, J.X., Wan, Y.S., Xu, Z.Q., Yang, J.S., Meng, F.C., 2001. Discovery of basic granulite and its formation age in Delingha area, North Qaidam Mountains. *Acta Petrologica Sinica* 17, 453–458.
- Zhang, J.X., Meng, F.C., Wan, Y.S., 2007. A cold Early Palaeozoic subduction zone in the North Qilian Mountains, NW China: petrological and U–Pb geochronological constraints. *Journal of Metamorphic Geology* 25, 285–304.
- Zhang, J., Gong, J., Yu, S., Li, H., Hou, K., 2013. Neoarchean–Paleoproterozoic multiple tectonothermal events in the western Alxa block, North China Craton and their geological implication: Evidence from zircon U–Pb ages and Hf isotopic composition. *Precambrian Research* 235, 36–57.
- Zhao, G., Cawood, P.A., 2012. Precambrian geology of China. *Precambrian Research* 222–223, 13–54.
- Zimmer, M., Kröner, A., Jochum, K.P., Reischmann, T., Todt, W., 1995. The Gabal Gerf complex: a Precambrian N-MORB ophiolite in the Nubian shield, NE Africa. *Chemical Geology* 123, 29–51.
- Zindler, A., 1986. Chemical geodynamics. *Annual Review of Earth and Planetary Sciences* 14, 493–571.